AGU PUBLICATIONS

JGR

Journal of Geophysical Research: Oceans

RESEARCH ARTICLE

10.1002/2017JC012801

**Key Points:**
- Simulation shows cascading happening from eastern Davis Strait
- The dense water formed on the shelf goes to deep Baffin Bay
- The event may be halted due to an increase in freshwater content on the WGS

**Correspondence to:**
J. M. Marson,
marson@ualberta.ca

**Citation:**
Marson, J. M., P. G. Myers, X. Hu, B. Petrie, K. Azetsu-Scott, and C. M. Lee (2017), Cascading off the West Greenland Shelf: A numerical perspective, *J. Geophys. Res. Oceans*, *122*, 5316–5328, doi:10.1002/2017JC012801.

Received 14 FEB 2017
Accepted 2 JUN 2017
Accepted article online 7 JUN 2017
Published online 3 JUL 2017



# Cascading off the West Greenland Shelf: A numerical perspective

**Juliana M. Marson[1], Paul G. Myers[1], Xianmin Hu[1], Brian Petrie[2], Kumiko Azetsu-Scott[2], and Craig M. Lee[3]**

[1]Department of Earth and Atmospheric Sciences, University of Alberta, Edmonton, Alberta, Canada, [2]Department of Fisheries and Oceans, Bedford Institute of Oceanography, Dartmouth, Nova Scotia, Canada, [3]Applied Physics Laboratory, University of Washington, Seattle, Washington, USA

**Abstract** Cascading of dense water from the shelf to deeper layers of the adjacent ocean basin has been observed in several locations around the world. The West Greenland Shelf (WGS), however, is a region where this process has never been documented. In this study, we use a numerical model with a 1/4° resolution to determine (i) if cascading could happen from the WGS; (ii) where and when it could take place; (iii) the forcings that induce or halt this process; and (iv) the path of the dense plume. Results show cascading happening off the WGS at Davis Strait. Dense waters form there due to brine rejection and slide down the slope during spring. Once the dense plume leaves the shelf, it gradually mixes with waters of similar density and moves northward into Baffin Bay. Our simulation showed events happening between 2003–2006 and during 2014; but no plume was observed in the simulation between 2007 and 2013. We suggest that the reason why cascading was halted in this period is related to: the increased freshwater transport from the Arctic Ocean through Fram Strait; the additional sea ice melting in the region; and the reduced presence of Irminger Water at Davis Strait during fall/early winter. Although observations at Davis Strait show that our simulation usually overestimates the seasonal range of temperature and salinity, they agree with the overall variability captured by the model. This suggests that cascades have the potential to develop on the WGS, albeit less dense than the ones estimated by the simulation.

## 1. Introduction

The production of dense waters on continental shelves is a fairly common process observed in high latitudes [*Ivanov et al*., 2004]. In those areas, surface waters lose heat during winter and become more saline due to the brine rejected from sea ice formation. Since continental shelves are often shallow, the cold and salty water is easily mixed to the bottom, producing a vertically homogeneous layer of dense waters. Once these dense waters have accumulated on the shelf, they form a plume that overflows and slides down the slope as a gravity current—an event known as *cascading* [*Cooper and Vaux*, 1949].

A cascading event can be generally divided into three main stages [*Shapiro et al*., 2003; *Ivanov et al*., 2004]. The first is the *preconditioning stage*, when dense water builds up on the continental shelf until it occupies the entire depth. Then there is the *main stage*, when the dense water forms a plume that flows down the slope. At this stage, the plume can be observed in a cross-shelf section as a near-bottom layer along the slope. The density at the maximum depth of the cascade is about the same as the density of shelf waters, and the isopycnal connecting both regions is possibly outcropping at the sea surface, which indicates that the dense water was formed locally rather than being advected from another place. The event ends at the *final stage*, when the waters from the cascade penetrate and mix with layers of same density.

Cascading enables direct exchange between surface and intermediate/deep layers of the ocean. Therefore, these shelf-basin exchanges may play an important role in forming deep and bottom water masses—which drive the Meridional Overturning Circulation (MOC)—as well as capturing carbon and other gases from the atmosphere [e.g., *Shapiro and Hill*, 2003; *Ivanov et al*., 2004]. *Ivanov et al*. [2004] compiled several cases of cascading around the world, which include observations made in Arctic and Antarctic seas. In the Southern Ocean particularly, cascading plays an essential role in the formation of the Antarctic Bottom Water [e.g., *Gordon et al*., 2009]. *Pickart et al*. [2005] pointed out the existence of a spill jet in East Greenland, the result

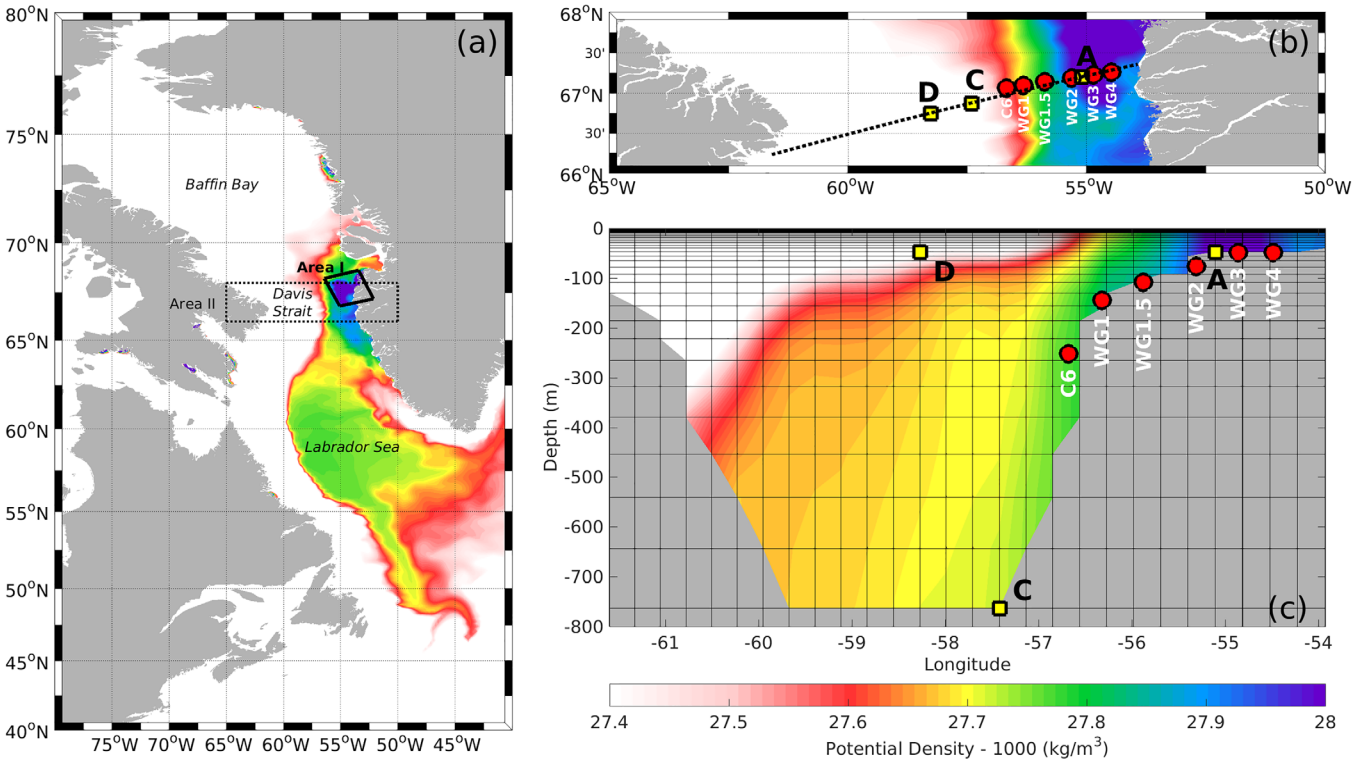


**Figure 1.** (a) The map on the left shows the area used for calculating averaged parameters over the West Greenland shelf (solid-line rectangle, Area I). (b) The detail on the top right is taken from Area II, indicated by the dashed-line rectangle on the left map, and shows the section used to present the vertical distribution of density and temperature. The detail also shows, horizontally, the locations of the three points (A, C, and D, yellow squares) used to calculate r and $R_0$ [*Ivanov et al.*, 2004] and the positions of the eastern moorings from *Curry et al.* [2014] (red circles). Finally, (c) the bottom right plot depicts the section indicated in detail above with the position of the points A, C, and D (yellow squares) and bottom-most sensors of the eastern moorings (red circles) through depth. The black lines show the model grid resolution. The colors in the figure indicate potential density anomaly from the simulation on 5 April 2004.

of cascading south of Denmark Strait. Nine years later, *von Appen et al.* [2014] argued that the spill jet is important to the MOC, since it provides waters of about the same density range as the Labrador Sea Water (a precursor of the North Atlantic Deep Water) to the northern North Atlantic. The question that remains open is if a similar feature exists on the West Greenland shelf (WGS).

Cascading off the WGS would also have the potential to impact the production of dense waters in the Labrador Sea, since it is in direct contact with it (see map in Figure 1). The west coast of Greenland also delimits Baffin Bay, which communicates with the Labrador Sea through Davis Strait. Therefore, depending on where the cascading occurred on the WGS, the dense water could impact either the Labrador Sea or Baffin Bay. In the latter case, if the plume were dense enough it could be trapped in the Bay because of the shallow sill in Davis Strait. Waters from the shelf, then, could be a source of Deep Baffin Bay Water, whose origin is still under discussion [*Tang et al.*, 2004].

Since cascading is intermittent and usually happens in higher latitudes during winter [*Ivanov et al.*, 2004] when the ocean is covered by sea ice, it is difficult to observe. A numerical simulation is, therefore, a useful tool to explore the possibility of shelf-basin exchange in such areas. In the present study, we use an ocean-sea ice coupled model to determine if cascading events occur off the West Greenland shelf. We then discuss the causes, the variability, and the fate of such events throughout the simulation (2002–2014).

## 2. Data and Methodology

The simulation analyzed in this study was carried out with the Nucleus for European Modelling of the Ocean [NEMO v3.4, *Madec and the NEMO Team*, 2008] model. The vertical grid is z-coordinate with partial steps, while the horizontal diffusion is Laplacian for tracers and bi-Laplacian for momentum, and the vertical turbulence is set by a turbulent kinetic energy (TKE) model. More detailed model parameters setup was

documented in *Dukhovskoy et al*. [2016]. The ocean model was coupled with the Louvain-la-Neuve Sea Ice Model (LIM2) [*Fichefet and Morales Maqueda*, 1997; *Bouillon et al*., 2009]. Outputs were saved as 5 day averages between 2002 and 2014. We used a 1/4° spatial resolution (from 27 km at the equator to 8 km in the Arctic) in a domain that comprises the Arctic and the Atlantic Ocean to 20°S—the ANHA4 configuration (http://knossos.eas.ualberta.ca/xianmin/anha/index.html), which originated from the ORCA025 grid [*Bernard et al*., 2006]. The first baroclinic Rossby radius on the WGS is much smaller than the ANHA4 resolution in this region, so the possible generation of eddies during cascading [e.g., *Lane-Serff and Baines*, 2000] cannot be resolved here. However, the absence of eddies is not detrimental for addressing the broad questions raised by this study. Moreover, the formation of the dense water showed in this study is well resolved at 1/4 degree resolution (around fifty grid points). The Canadian Meteorological Centre's global deterministic prediction system reforecasts (CGRF) [*Smith et al*., 2014] were used to force the simulation (hourly fields with 33 km resolution). Initial and open boundary conditions were taken from the Global Ocean Physics Reanalysis (GLORYS2v3) [*Masina et al*., 2015]. The simulation also included Greenland meltwater fluxes provided by *Bamber et al*. [2012].

Our analyses use the outputs of the simulation for the area, section, and points indicated in Figure 1. The area delineated by the smaller square in Figure 1 (Area I), was used to calculate vertical transport, sea ice production, concentration and thickness, freshwater content, and tracer concentration on the eastern shelf of Davis Strait. The section across Davis Strait was used to calculate the average potential temperature, salinity, and density close to observation points and to show the vertical density and temperature distribution in the area. The points labeled A, C, and D (Figure 1, right) were used to calculate the cascading parameters $r$ and $R_0$ described by *Ivanov et al*. [2004] and presented below. Throughout this paper, we will often use the year of 2004 as a reference period for cascading events. The choice of this specific year will become clear when we present the vertical transport of dense water across 200 m in Area I.

*Ivanov et al*. [2004] place five key points along the vertical cross-slope section that depicts a cascading event:

A: point placed at the maximum density ($\rho_A = \rho_{max}$) in the cascade (usually over the continental shelf);
B: point at depth (outside the plume) that has the same density as the descending dense water ($\rho_B = \rho_A$);
C: point placed at the density minimum between A and B ($\rho_C = \rho_{min}$), marking the position of the plume edge;
D: point located in the ambient water (undisturbed by the plume) at the same depth as A; and
E: point at the intersection of the isopycnal in C and the vertical line from point B.

For our purposes, A, C, and D are the only relevant points because there is no layer in the water column with the same density as the shelf water during cascading events (no point B). In this case, since the density decreases monotonically down-slope, C was placed at the deepest point of the slope (Figure 1c).

*Ivanov et al*. [2004] defined the parameter

$$r = \frac{\rho_A - \rho_C}{\rho_A - \rho_D} \tag{1}$$

which indicates the development stage of the cascading event by differences of density among the shelf water ($\rho_A$), the ambient water ($\rho_D$), and the water at the bottom of the slope ($\rho_C$) (Figure 1c). At the preconditioning stage, $r$ would be close to 1, since the density of the shelf waters is significantly higher than both ambient and bottom water density. As the shelf waters progress down the slope, the density difference between the waters over the shelf and those at the bottom of the slope decreases, so $r$ approaches zero. During the months when none of the cascading stages takes place, shelf water density is not very different from the ambient water density, leading to large $r$ values.

An additional parameter, $R_0$ [*Ivanov et al*., 2004], indicates the relative importance of temperature and salinity to the cascading event. $R_0$ is defined as

$$R_0 = \frac{\alpha(T_A - T_D)}{\beta(S_A - S_D)} \tag{2}$$

where $\alpha$ and $\beta$ are the coefficients of thermal expansion and salinity contraction, respectively, and T and S are temperature and salinity at the indicated points. Small $R_0$ values indicate cascades driven mainly by salinity differences, while large $R_0$ values point to cascades driven by temperature differences.

The freshwater content (FWC) of Area I is given by

$$FWC = \int\int\int_{z=0}^{h} \frac{S_{ref} - S}{S_{ref}} \, dx \, dy \, dz \tag{3}$$

where $x$ and $y$ denote longitude and latitude, respectively; $z = 0$ is the surface and $h$ is the deepest level of a given grid point; $S$ is the salinity of the grid point; and $S_{ref}$ is 34.8 [*Aagaard and Carmack*, 1989].

In order to evaluate the path of the plume, we used a Lagrangian tool called ARIANE [*Blanke and Raynaud*, 1997; *Blanke et al*., 1999]. Given the output temperature, salinity, and velocity fields from our simulation, ARIANE was able to track 3000 particles released from Area I (indicated in Figure 1a) over 18 months. The particles were initially placed randomly inside the volume of Area I in early March 2004. The position, temperature, and salinity of each particle were then recorded every five days until September 2005.

Hydrographic observations between 2004 and 2011 were provided by a moored array (Figure 1b) and by CTD profiles collected at the mooring sites during deployment and recovery cruises [*Curry et al*., 2011, 2014; *Azetsu-Scott et al*., 2012; *Punshon et al*., 2014]. Sea ice concentration data were obtained by the AMSR-E sensor [*Cavalieri et al*., 2014].

## 3. Results and Discussion

Since the source of dense waters that form cascades is usually local, shelf regions of anomalously dense surface waters can indicate potential cascading events [*Ivanov et al*., 2004]. Figure 2a shows an example of such a surface signature, taken from April 2004 outputs. The eastern Davis Strait is covered by dense water (in dark blue/purple, around 28 kg/m$^3$) while its surrounding ambient waters are relatively less dense (around 27.4 kg/m$^3$). The same feature appears in the near-bottom density field (Figure 2b), which indicates that the dense water occupies the entire depth on the eastern Davis Strait shelf. This area is the most persistent and significant source of dense waters on the entire WGS during winter and spring throughout the simulation period.

We assessed the simulation's robustness at Davis Strait by comparing observations made by WG moorings indicated in Figure 1 and the simulation values in the points closest to these moorings. Figure 3 shows monthly means of potential temperature, salinity, and potential density anomaly. The simulation time series (red lines) correlate with the observations (blue circles) with coefficients of 0.93 (temperature), 0.66 (salinity), and 0.81 (density). The range of these time series is often overestimated by the model (see minimum and

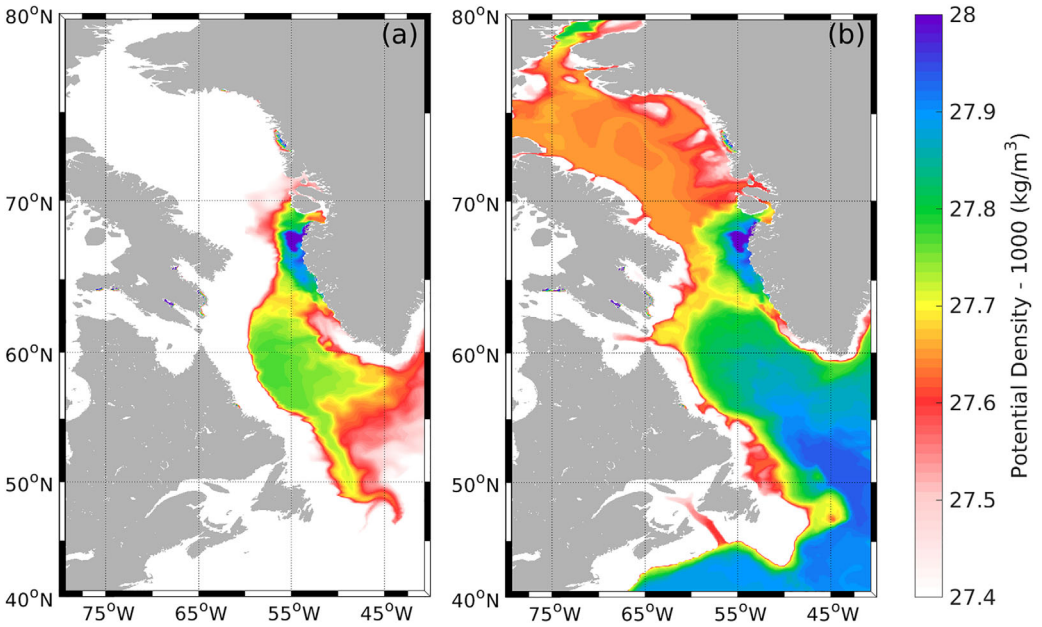


**Figure 2.** Potential density anomaly from the simulation (a) at the surface and immediately above the bottom (b) on 5 April 2004.

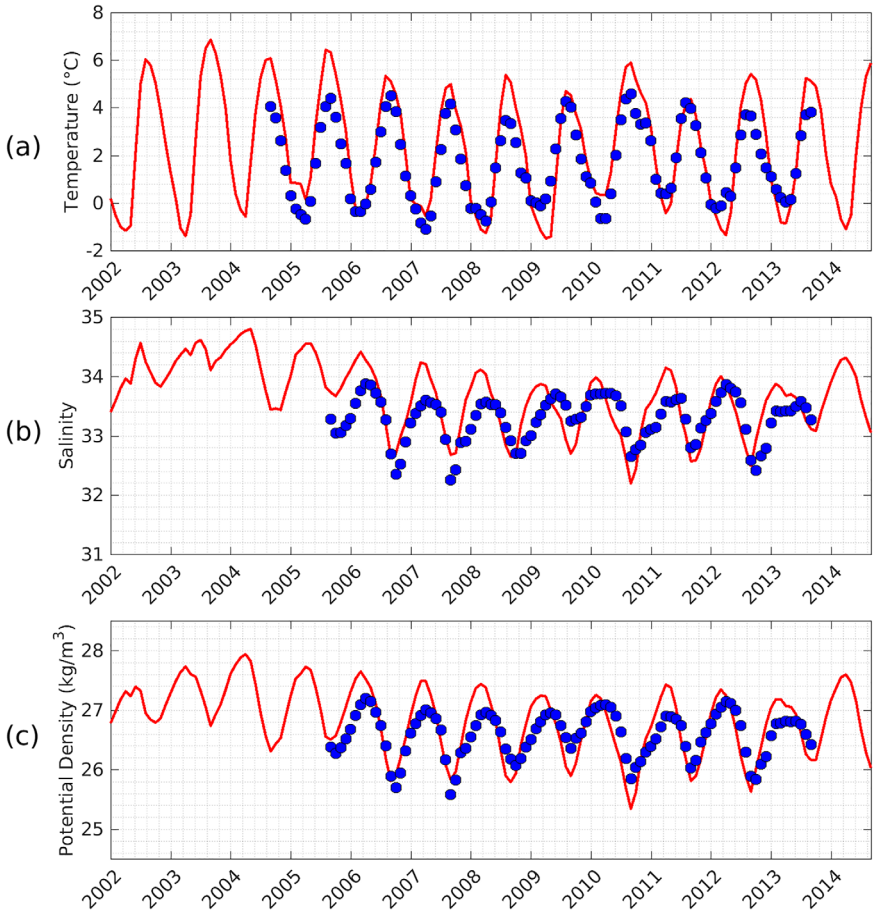


**Figure 3.** Monthly evolution of (a) potential temperature, (b) salinity, and (c) potential density anomaly in the simulation (red lines), and in the WG mooring records (blue circles). Simulation values (red line) are averages for points in the section indicated in Figure 1b that are closest to the WG mooring locations. Both simulated and observed time series were averaged throughout the entire water column.

maximum values in Table 1 for details) and the salinity time series is slightly out of phase. To be more accurate, we fit the model and observations time series to a mean and an annual harmonic given by

$$A_0 + A_1 * cos(2\pi(t-\phi)/12) \quad (4)$$

We found out that the annual temperature, salinity, and density cycles' amplitudes are overestimated by 38%, 39%, and 57%, respectively; they are almost in phase for temperature, but salinity and density are out of phase by over a month (see Table 1). The overestimation and lag of the salinity time series could be related to the way sea ice grows inside the analyzed region in the model (see further discussion at the end of this section).

**Table 1.** Minimum, Maximum, Average ($A_0$), Amplitude ($A_1$), and Phase ($\phi$) of the Time Series Presented in Figure 3 From Mid-2005 to Late-2013[a]

| | Minimum | | Maximum | | Average ($A_0$) | | Amplitude ($A_1$) | | Phase ($\phi$) | |
|---|---|---|---|---|---|---|---|---|---|---|
| | SIM | OBS | SIM | OBS | SIM | OBS | SIM | OBS | SIM | OBS |
| $\theta$ | −1.50 | −1.11 | 6.43 | 4.58 | 2.27 | 1.66 | 2.99 | 2.17 | −2.92 | −3.12 |
| $S$ | 32.19 | 32.25 | 34.41 | 33.88 | 33.46 | 33.28 | 0.61 | 0.44 | 3.13 | 4.46 |
| $\sigma$ | 25.34 | 25.58 | 27.65 | 27.19 | 26.69 | 26.59 | 0.72 | 0.46 | 3.12 | 4.01 |

[a]SIM = simulation; OBS = mooring observations; $\theta$ = potential temperature (°C); $S$ = salinity; $\sigma$ = potential density – 1000 (kg/m$^3$).

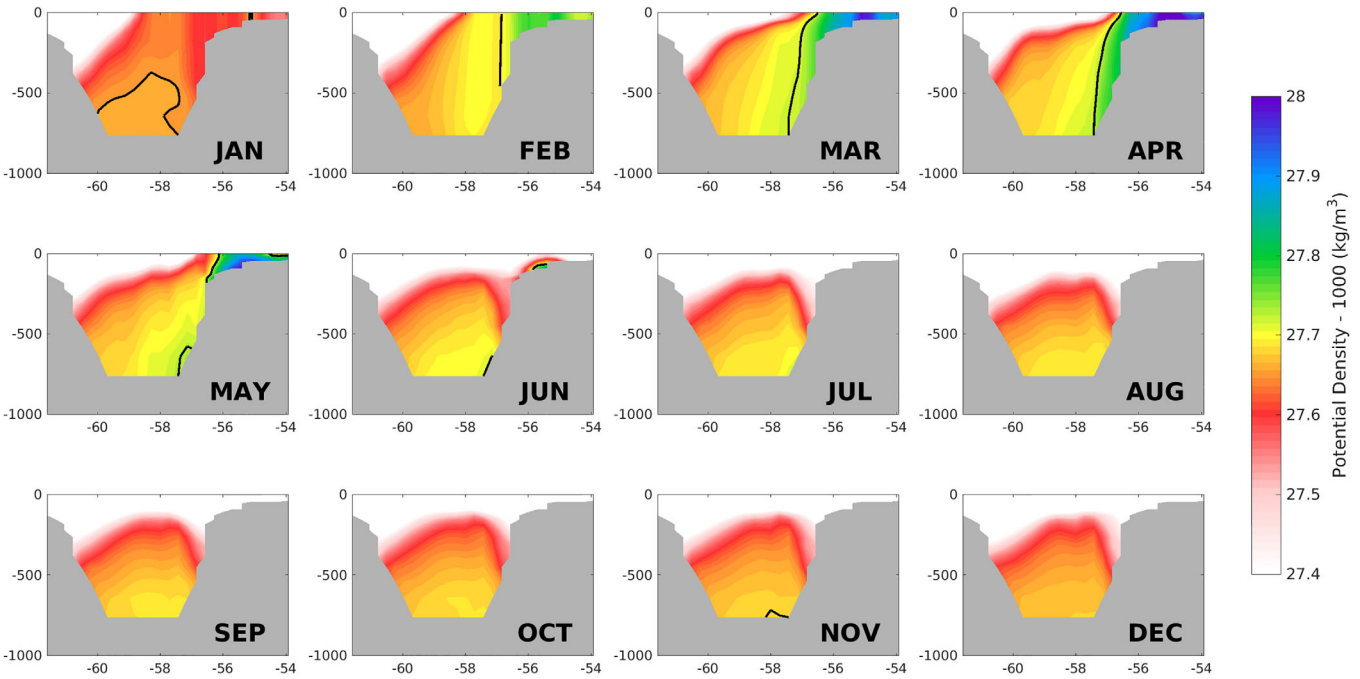


**Figure 4.** Monthly averaged potential density anomaly for 2004 in the section indicated by Figure 1b. The black line shows the location of the isopycnal passing through point C (indicated in Figure 1c).

The most striking feature from the simulation time series (red line in Figure 3) is that the average salinity (and, therefore, the potential density anomaly) between 2002 and 2006 does not have a minimum around October as low as the ones we observe for the following years. Also, the maximum salinities in winter for this period are generally higher. This change in amplitude could be an initialization problem within the simulation but we argue against it since (i) the simulation would not take that long to stabilize in the upper ocean; (ii) the usual model temporal drift in this region is toward increasing salinities [e.g., *Rattan et al.*, 2010], which is the opposite of what we see; and (iii) the temperature variability for the same area does not show the same change in amplitude or any other signs of model adjustment. Moreover, although the observations of salinity start only in September 2005 (blue circles in Figure 3b), they show a similar size decrease in minimum salinity between 2005 and 2006, indicating that the model captured this trend.

The simulated seasonal variation of density suggests that a preconditioning stage could be happening from December through February, when the Area I average density increases to 27.5–28 kg/m$^3$ (Figure 3c). Figure 4 shows how the seasonal variation of density progresses spatially in 2004 at the cross-shelf section indicated in Figure 1b. Indeed, the densities on the eastern shelf are higher in February, and a dense plume slides down the slope between March and May. The black line, which indicates the position of the isopycnal passing through point C, also provides valuable information: it shows when the density of the bottom is the same as over the shelf, which suggests that the water from the shelf is reaching the bottom of the slope. Moreover, the outcrop of this isopycnal at the surface between February and May (added to the isolated characteristic of the dense "blob" at the surface in Figure 2a) indicates that the dense water present on the shelf was transformed locally through atmosphere-ocean interactions [*Ivanov et al.*, 2004].

Since the density variation is clearly seasonal, could we assume that cascading is also seasonal and, thus, happens every year? To answer this question, we have calculated the cascading parameters and the vertical transport of dense water (higher than 27.7 kg/m$^3$) across 200 m inside Area I (Figure 5). As explained in the Methodology section, the cascading parameter $r$ indicates the stage of development of the cascade. When the process happens, $r$ should be between 1 and 0, indicating that the density of waters over the shelf is very close to the density of waters down the slope, but quite different from the ambient water density [*Ivanov et al.*, 2004]. Meanwhile, if $R_0$ is near zero during a cascading event, this event is probably driven by salinity differences; if $R_0$ is large, temperature differences must be more important in creating a density contrast and triggering cascading [*Ivanov et al.*, 2004].

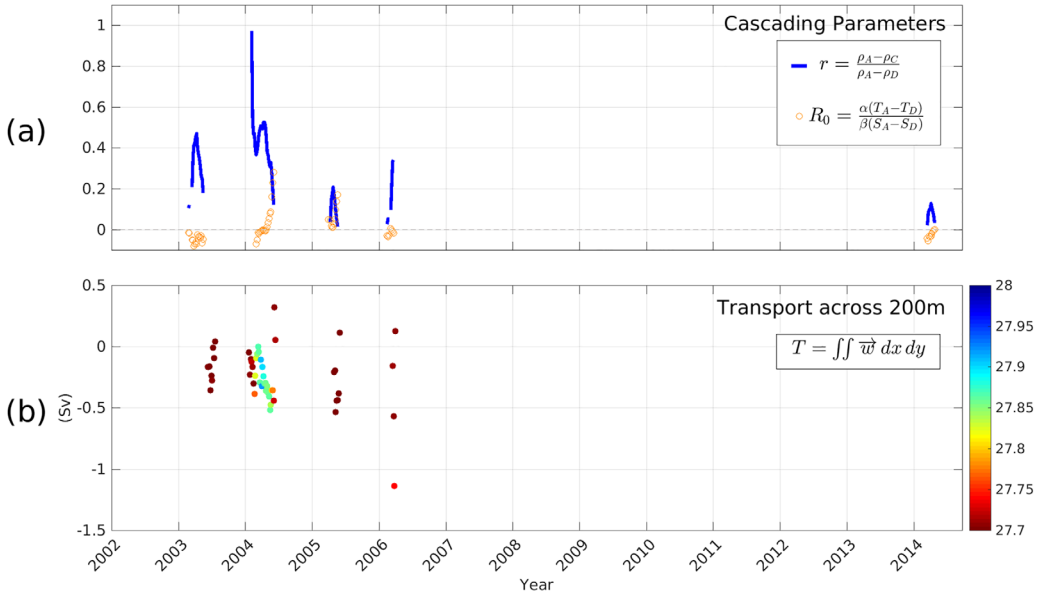


**Figure 5.** (a) Cascading parameters r (blue line) and $R_0$ (orange circles) as defined by *Ivanov et al.* [2004] and described in the Methodology section. Only values in the interval $0 \leq r \leq 1$ are shown. (b) Transport of waters denser than 27.7 kg/m$^3$ across the 200 m isobath in Area I (see Figure 1). Negative values indicate downward movement. The points' colors indicate the average density of the transported water.

Figure 5a shows the parameters $r$ and $R_0$ between 2003–2006 and in 2014, when $r$ indicates cascading events ($0 \leq r \leq 1$). $R_0$ values are close to zero, which implicate salinity as the primary source of density differences between shelf water and ambient water, leading to the instability that drives the dense water down the slope. Another way to confirm that cascading was happening during those years is to look at the vertical transport of dense waters (density higher than 27.7 kg/m$^3$) across 200 m in Area I. If the transport is negative, it means that dense water is crossing the 200 m isobath downward. Once again, this downward transport only happens between 2003 and 2006. The absence of any transport in 2014, when cascading parameters indicate a weak event, happens because the water sliding down the slope at that time was lighter than 27.7 kg/m$^3$ (around 27.6 kg/m$^3$). The event in 2004 seems to have been the most intense one, with denser waters (between 27.85 and 27.90 kg/m$^3$) being transported for a longer period. That is the reason why we chose the year of 2004 to exemplify a cascading event off the WGS.

So far we showed that: (i) cascading happens off the WGS in the simulation; (ii) it usually takes place during winter and spring (between February and May); and (iii) it does not happen every year; rather it is a sporadic and intermittent event, as pointed out in previous studies [e.g., *Ivanov et al.*, 2004; *Shapiro et al.*, 2003]. We also showed that the events are driven by differences in salinity between shelf water and ambient water. But what causes those differences and, ultimately, generates a down slope flux of dense water off the WGS? Two of the most common physical mechanisms that lead to cascading in high latitude areas are heat loss to the atmosphere and salinization during sea ice formation (and associated brine rejection). As Figure 5a indicated, cascading events in the studied area are driven by differences in salinity; therefore, brine rejection is the most promising process to explain why cascading would happen there. Thus, we analyzed the sea ice concentration and thickness over the area of interest. Figure 6 presents the simulated (left map) and observed (right map) sea ice concentrations for March 2004 and the monthly averaged sea ice concentration and thickness for Area I (bottom plot).

The area we selected is partially covered by sea ice from January through May, when brine rejection would lead to an increase in the density of surface waters. In fact, comparing the simulated sea ice cover in this area (Figure 6, top left) with the surface density in the same area (Figure 2), one can see that the edge of the sea ice cover is very similar to the edge of the high surface density "blob," which adds to the evidence that brine rejection is the primary process forcing cascading off the WGS. Although the satellite data show a continuous sea ice cover from west into Area I (Figure 6 top right) instead of the simulated "blob," they point to even higher concentrations of sea ice in this during the same months. This suggests that, if other physical conditions are similar to the model ones, cascading events in this region are realistic.

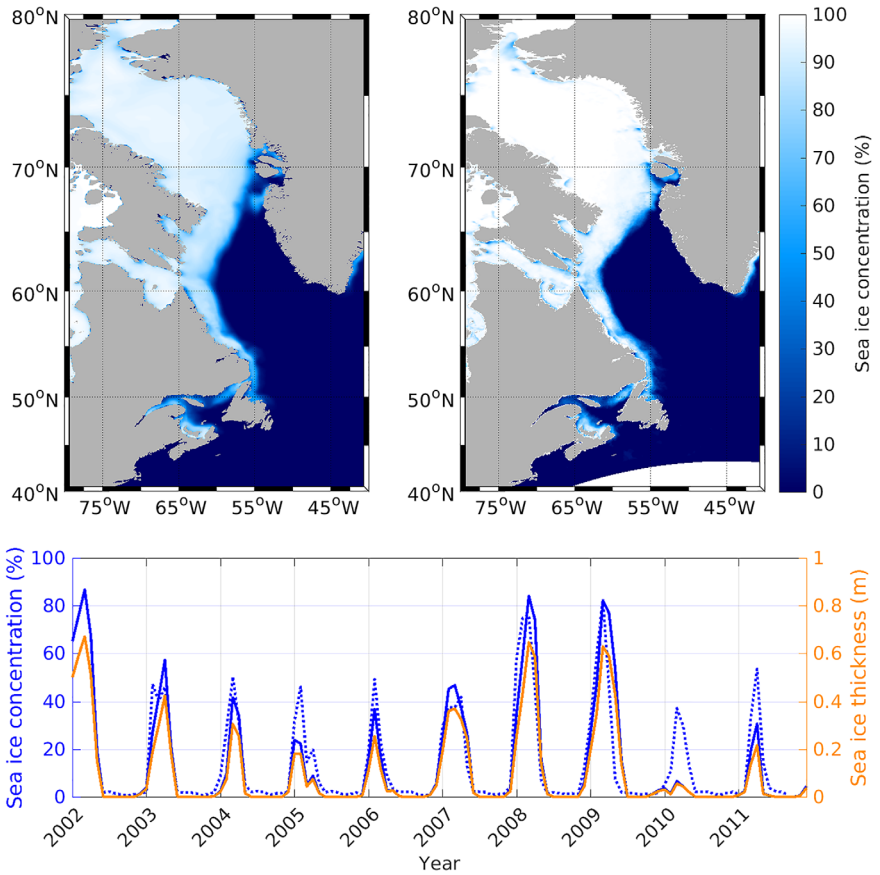


**Figure 6.** The top maps show sea ice concentration (%) averaged for March 2004 as seen from the simulation (left) and from AMSR-E (right). The bottom plot shows the monthly averaged sea ice concentration (blue) and thickness (orange) for Area I. The solid lines represent simulation values, while the dotted blue line represents averaged sea ice concentration from AMSR-E.

If sea ice formation triggers the cascading events on the WGS, why does this process not take place after 2007, when sea ice concentration is even higher than between 2003 and 2006 (as shown by Figure 6, bottom plot)? To answer this question, we need to go back to the salinity time series presented in Figure 3. As pointed out before, the area analyzed showed higher maxima and higher minima throughout the seasonal cycle of salinity from 2002 until the first half of 2006. After that, the amplitude of the salinity variability increases, and the minimum salinity decreases by ~1. Figure 7b shows that the freshwater content of Area I increased significantly after the middle of 2006, which explains the decrease in salinity and the halt in cascading events: the increased freshwater content on the shelf reduces the density difference between shelf waters and their surroundings, and this reduced difference is not enough to generate a gravity current. We first checked if this freshwater increase could be related to an increased melting of the Greenland ice sheet. As the simulation included a passive tracer to track Greenland meltwater, the amount of tracer inside Area I was examined (Figure 7c). Although there is a slight increase in Greenland meltwater from 2005 to 2007, this increase does not seem enough to result in the much more drastic difference in freshwater content between 2005 and 2006.

The second step was to check the sea ice production in the area (Figure 7d). As seen in Figure 6, the amount of sea ice formed between 2005 and 2007 did not change much (it actually increased slightly). But Figure 7d reveals something else. As indicated by the smaller negative peak (ice melt) compared to the positive peak (ice production) between 2004 and the end of 2006, sea ice formed inside Area I was apparently advected from the region and melted elsewhere. In 2007, however, the amount of melted sea ice was even larger than what was formed in the area, resulting in a freshwater import. The imbalance between sea ice freezing and melting must certainly affect the freshwater content inside Area I; however, the additional meltwater entered the ocean only in the spring of 2007, while the increase in freshwater content happened in the second half of 2006. We, then, looked for other freshwater sources to the area.

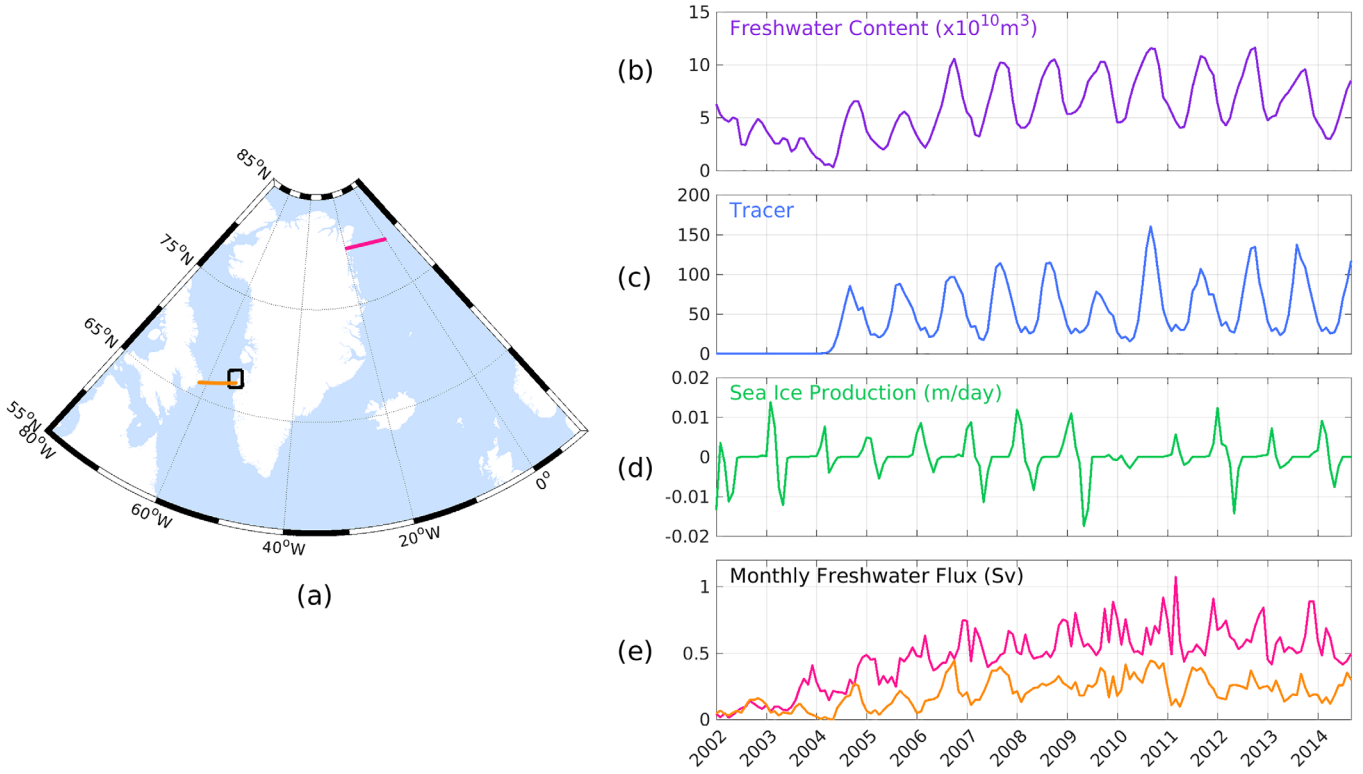


**Figure 7.** (a) Map showing the area (black, same as Area I from Figure 1) used to calculate freshwater (and tracer) content and sea ice production; and sections (pink and orange) used to calculate freshwater flux. (b) Monthly averaged freshwater content inside Area I. (c) Amount of Greenland meltwater tracer inside Area I. The tracer was introduced in the simulation in 2004. (d) Monthly averaged sea ice production inside Area I. Positive values indicate freezing, while negative ones indicate melting. (e) Monthly freshwater flux normal to the sections at Fram Strait (southward, pink line) and at Davis Strait (northward, orange line).

The next tested explanation for the 2006 increase in freshwater content was the incoming Arctic freshwater brought by the West Greenland Current. Figure 7e shows the southward freshwater flux at Fram Strait (pink) and the northward freshwater flux at Davis Strait (orange). The two time series covary with Davis Strait lagging Fram Strait by almost a year (correlation of 0.61). This is consistent with the amount of time that waters take to go around Greenland (estimated in our simulation through a passive tracer leaving Fram Strait). The southward freshwater flux at Fram Strait increases from 2002 to 2010 in the simulation, and it seems to stabilize after that. At Davis Strait, the northward freshwater flux increased more significantly at the end of 2006 and then varies around the same range until 2012, when the freshwater flux is slightly reduced (which may be the reason why there is a cascading event again in the simulation in 2014). Using observations, *Rabe et al*. [2013] and *Haine et al*. [2015] have not observed such a trend in Fram Strait's freshwater flux. However, *Rabe et al*. [2013] show that freshwater flux was smaller in September 2010 compared to previous years, which fits the possibility that cascading could have happened at Davis Strait in 2012, as we will discuss later (Figure 11).

Since the northward freshwater transport at Davis Strait is not entirely explained by the increased inflow of fresh Arctic waters, we analyzed the possibility of a decreased influx of salty waters in 2007. Besides the cold and fresh water with Arctic origins, the West Greenland Current also brings warm and salty Irminger Water to the region [*Fratantoni and Pickart*, 2007], especially during winter. *Curry et al*. [2014] define the West Greenland Irminger Water (WGIW) by temperatures and salinities greater than 2°C and 34.1, respectively. Figure 8 shows the averaged temperature in January at Davis Strait (section shown in Figure 1b) for 2004 and 2007. Observe that the yellow-to-red range shows waters warmer than 2°C, and the dotted black line shows the 34.1 isohaline (waters below this line are saltier). From this figure we can see a larger WGIW core at Davis Strait shelf break in 2004 compared to 2007. Additionally, the wind stress, which is predominantly southward during winter in this region, is stronger and has a more persistent direction in 2004 than in 2007 (see inserts in Figure 8). Considering that winds blowing southwards are upwelling favourable on the WGS, those winds probably contributed to bringing Irminger Water from the shelf break to the shelf.

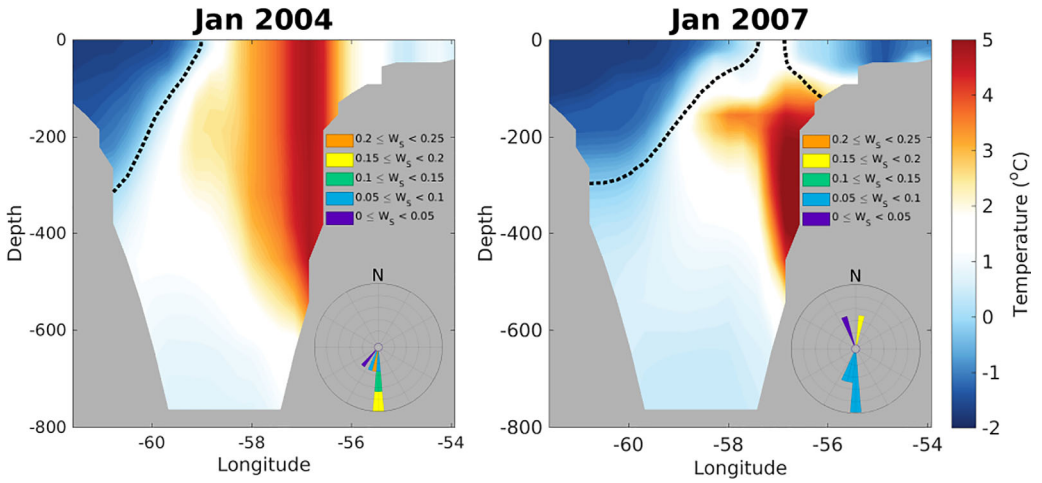


**Figure 8.** January averages of potential temperature for 2004 (left), and 2007 (right) in the section depicted in Figure 1b. The dotted black line indicates salinity of 34.1, while the inserts indicate the wind stress direction relative to the section for January 2004 and 2007 in Area I. In those inserts, the size of the bar indicates the frequency with which the wind stress was observed to point to that direction, and the colors indicate the strength of the wind stress.

This scenario could have preconditioned shelf waters to be saltier in 2004 compared to 2007. Moreover, *Myers et al*. [2007, 2009] show that a larger volume of Irminger Water was transported through West Greenland sections in the early 2000s. Since the maximum influx of WGIW at Davis Strait occurs between October and December [*Curry et al*., 2014], the reduced presence of this water mass around those months would relatively increase the freshwater content of the area compared to years with strong WGIW presence—which agrees with the sudden increase of freshwater in late-2006.

We have shown that, in our simulation, cascading happens sporadically on the WGS. Dense water is formed over the shelf through salinization due to sea ice formation during winter/early spring and, if the freshwater content is limited, the shelf water becomes dense and voluminous enough to slide down the slope. Regarding the fate of this plume, we used the offline Lagrangian tracking tool, ARIANE, to track the 3-D trajectory of each particle released in a given area. We inserted 3000 particles in Area I (Figure 1) in early March 2004 and observed their trajectories up to September 2005. Figure 9 shows the trajectories of particles that, at some point, moved to depths below 500 m. The particles that sank in Davis Strait entered some troughs along the WGS and flowed toward Baffin Bay, where they became trapped in the deep gyre of this basin. The density of the particles decreases as they mix with other water masses and their final density is about 27.6 kg/m$^3$, which is consistent with the observed density of Baffin Bay Deep Water [*Münchow et al*., 2015].

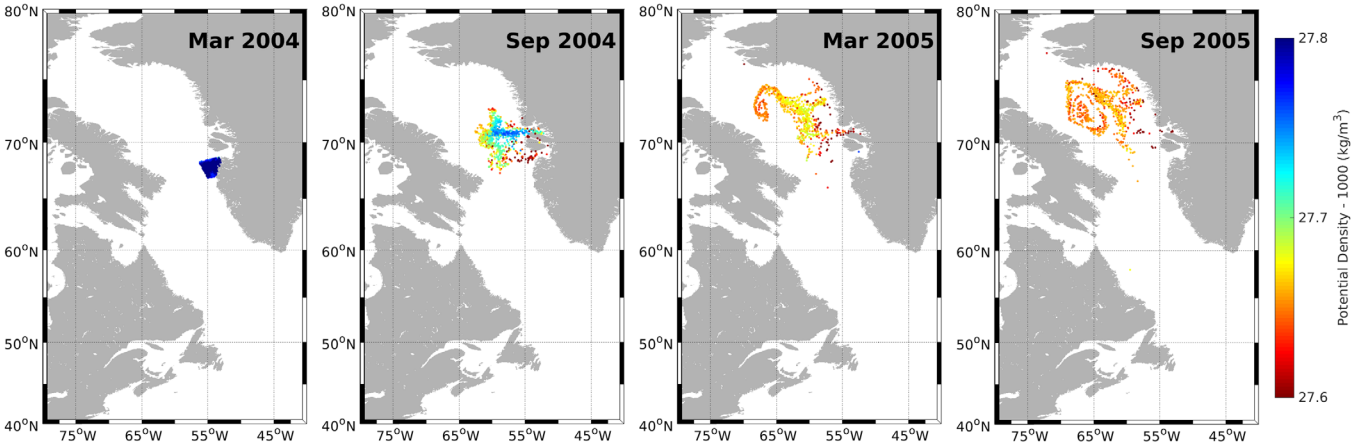


**Figure 9.** Trajectories of particles released inside Area I (Figure 1a) between March 2004 and September 2005. The points show only particles that, at some point, reached 500 m or deeper. The color indicates the density of each particle.

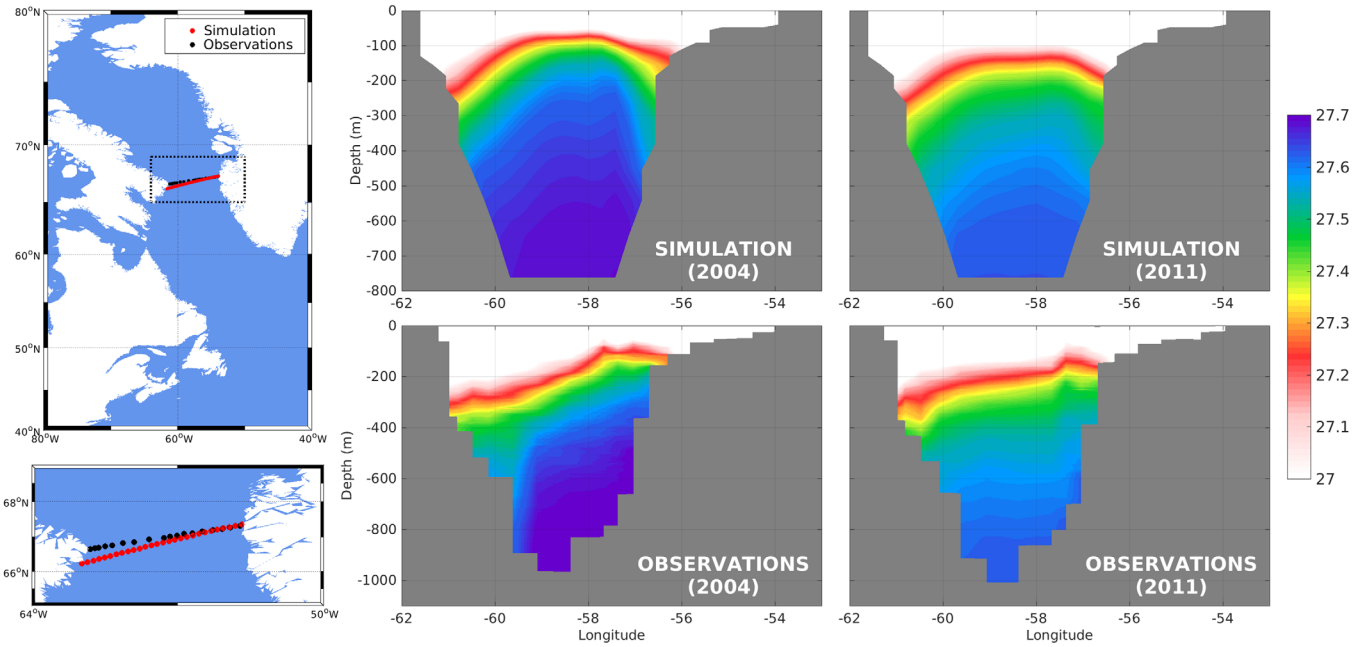


**Figure 10.** Comparison between density fields from the simulation and observations. The larger map and detail on the left show the location of the simulation transect (red) in relation to CTD stations (black). On the right, the plots show averaged density in September/early October 2004 (left) and 2011 (right) for the simulation (top) and observations (bottom).

The contribution of these dense plumes to the formation of Baffin Bay Deep Water, however, appears to be very small. In 2004, for instance, the total volume exported (according to results shown in Figure 5b) was around $3.1 \times 10^{12}$ $m^3$—which is 1% of Baffin Bay volume below 500m (around $2.9 \times 10^{14}$ $m^3$).

In terms of spatial distribution of properties, we compare our simulation results with CTD data from *Azetsu-Scott et al.* [2012] and *Punshon et al.* [2014], since those provide a better spatial coverage along the Davis Strait section when compared to the mooring records. Figure 10 presents the density fields averaged from September to early October. Those months are not ideal to observe cascading events since they should be over by then, but a reflection of the plume's characteristics should be seen in the bottom of the Strait. Although the shape of the isopycnals are somewhat different on the west side because the Baffin Island Current is more intense and spatially confined in the model, the range of densities is the same for both observations and simulation. Previously, we have seen that 2004 was a year where cascading was particularly significant in this region because shelf waters were dense enough to overflow. In contrast, in 2011 cascading was absent because the freshwater content on the shelf hindered the dense plume formation. Here, we notice that observations show denser waters at the bottom of the Strait in 2004 compared to 2011—just as seen in the simulation section.

The best way to determine if a cascading event happened during the mooring records would be to calculate the *r* parameter using different sensors over the shelf, on the bottom of the slope, and in the middle of the Strait. However, the sensors are not positioned in the same A, C, and D points described in section 2 (see Figure 1c), so we plotted the density of the bottom-most sensor of each mooring on the eastern Davis Strait shelf separately (Figure 11). In April 2006, the shelf waters (WG2 and WG3) appear to reach at least the shelf break (WG1). In the following years, however, those shelf waters are not as dense (less than 27 kg/$m^3$) and differ significantly from waters at the shelf break (WG1) and slope (C6), indicating once more that cascading was more likely to happen before mid-2006. An exception is 2012, when shelf waters appear to reach the slope again—although our simulation did not capture any cascading event then. Interestingly, the dense waters seem to form in the middle of the shelf, away from the coast, since the WG4 sensor usually displays lower densities compared to WG2 and WG3. This brings us again to the differences of sea ice concentration between the model and the satellite images: the observed sea ice cover seems to spread from west and do not reach the coast, while the simulation appears to create sea ice from the coast out. This could be the reason why the salinity time series in Figure 3 have slightly different ranges and phases.

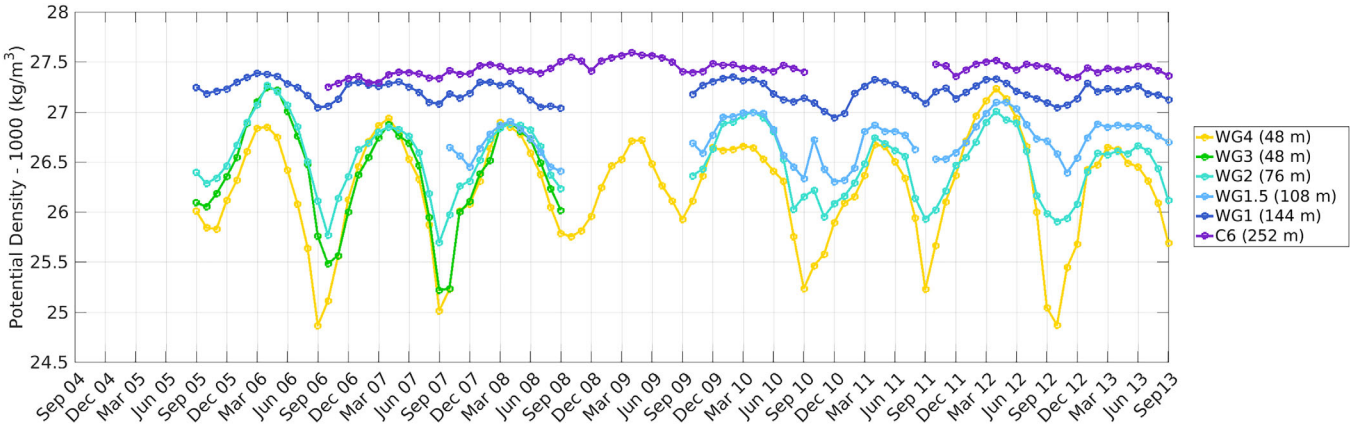


**Figure 11.** Density from the bottom-most sensors in the eastern moorings at Davis Strait.

We also compared both studies carried out by *Curry et al*. [2011, 2014]. While *Curry et al*. [2011] presents the monthly average from 2004 to 2005, *Curry et al*. [2014] show the averages for the period of 2004–2010. Again, the average salinity over the WGS is higher for the 2004–2005 period (maximum of ∼34) than for the 2004–2010 period (maximum of ∼33.5). Moreover, in both studies the 27 kg/m$^3$ isopycnal outcrops on the WGS during the indicated cascading months, suggesting that there may have been a direct communication between the surface and deep Davis Strait at this time. In *Curry et al*. [2011], the outcrop lasts longer (from January to June) than in *Curry et al*. [2014] (from April to June) also pointing toward a more intense shelf-basin exchange during 2004–2005 compared to later years.

## 4. Summary and Final Considerations

The present study revealed that cascading—a process in which dense waters formed on the continental shelf slide down the slope and become part of intermediate and deep layers—may be observed on the West Greenland Shelf (more specifically, around Davis Strait), based on the analyses of an ice-ocean numerical simulation. These analyses showed that:

1. A dense plume is generally formed in this area around February and March (preconditioning stage);
2. The plume flows down the slope between March and May (main stage) and ends up in Baffin Bay;
3. Cascading does not happen every year: it was observed in the simulation between 2003 and 2006—with a particularly strong event in 2004—and later in 2014;
4. The main factor that drives the dense water formation over the shelf is the increase in salinity resulting from sea ice formation during winter in the eastern part of Davis Strait;
5. Cascading may be halted if (a) freshwater coming from the Arctic through Fram Strait was particularly large in the previous year; (b) there is more sea ice melting than freezing in the area; and (c) Irminger Water influx and upwelling onto the shelf was not particularly strong during fall and early winter; and
6. Since key features of our simulation represent Davis Strait conditions reasonably well when compared to observations, cascades have the potential to develop in this region, although with lower densities than suggested by the model.

As for every numerical study, the present one also has its limitations. The two most relevant ones are: (i) the model does not take tides in account, which provide additional turbulence that facilitates downslope propagation [*Shapiro and Hill*, 1997] and dilution [*Wobus et al*., 2013] of the plume; and (ii) the liquid freshwater input from the Greenland ice sheet, which is used as a boundary condition in our simulation, represents only 46% of the total freshwater delivered to Greenland's surroundings [*Bamber et al*., 2012]. The remaining 54% is in solid form and is not implemented in the simulation used in this study. *Marsh et al*. [2015] showed that Davis Strait and Disko Bay surface salinity was reduced by 0.1–0.2 when icebergs were included in their simulations. This surplus of freshwater has the potential to hinder or change cascading events in the area. Both issues are currently being addressed by our group and we hope to have soon a simulation with working tides and an interactive iceberg component.

**Acknowledgments**
For access to the model data contact P.G. Myers (pmyers@ualberta.ca). For the observations at Davis Strait, access https://arcticdata.io or http://iop.apl.washington.edu. We gratefully acknowledge the financial and logistic support of grants from the Natural Sciences and Engineering Research Council (NSERC) of Canada (RGPIN 04357 and RGPCC 433898), as well as Polar Knowledge Canada (PKC-NST-1617–0003). We are grateful to the NEMO development team and the Drakkar project for providing the model and continuous guidance, and to Westgrid and Compute Canada for computational resources. We would also like to thank G. Smith for the CGRF forcing fields and G. Garric for the GLORYS2v3 output. Greenland freshwater flux data analyzed in this study are presented in *Bamber et al*. [2012] and are available on request as a gridded product. Craig M. Lee also thanks the NSF Arctic Program for the grants ARC1022472, ARC0632231, and OPP0230381, which supported his involvement in this project and the observations used here.

## References

Aagaard, K., and E. C. Carmack (1989), The role of sea ice and other fresh water in the Arctic circulation, *J. Geophys. Res.*, *94*, 14,485–14,498, doi:10.1029/JC094iC10p14485.

Azetsu-Scott, K., B. Petrie, P. Yeats, and C. Lee (2012), Composition and fluxes of freshwater through Davis Strait using multiple chemical tracers, *J. Geophys. Res.*, *117*, C12011, doi:10.1029/2012JC008172.

Bamber, J., M. Van Den Broeke, J. Ettema, J. Lenaerts, and E. Rignot (2012), Recent large increases in freshwater fluxes from Greenland into the North Atlantic, *Geophys. Res. Lett.*, *39*, L19501, doi:10.1029/2012GL052552.

Bernard, B., et al. (2006), Impact of partial steps and momentum advection schemes in a global ocean circulation model at eddy-permitting resolution, *Ocean Dyn.*, *56*(5), 543–567, doi:10.1007/s10236-006-0082-1.

Blanke, B., and S. Raynaud (1997), Kinematics of the Pacific Equatorial Undercurrent: An Eulerian and Lagrangian approach from GCM results, *J. Phys. Oceanogr.*, *27*, 1038–1053, doi:10.1175/1520-0485(1997)027 < 1038:KOTPEU>2.0.CO;2.

Blanke, B., M. Arhan, G. Madec, and S. Roche (1999), Warm water paths in the Equatorial Atlantic as diagnosed with a General Circulation Model, *J. Phys. Oceanogr.*, *29*(11), 2753–2768, doi:10.1175/1520-0485(1999)029 < 2753:WWPITE>2.0.CO;2.

Bouillon, S., M. Morales Maqueda, V. Legat, and T. Fichefet (2009), An elastic-viscous-plastic sea ice model formulated on Arakawa B and C grids, *Ocean Modell.*, *27*, 174–184, doi:10.1016/j.ocemod.2009.01.004.

Cavalieri, D. J., T. Markus, and J. C. Comiso (2014), *AMSR-E/Aqua Daily L3 6.25 km 89 GHz Brightness Temperature Polar Grids*, Version 3. NASA Natl. Snow and Ice Data Cent. Distrib. Active Arch. Cent., Boulder, Colo., doi:10.5067/AMSR-E/AE_SI6.003.

Cooper, L. H. N., and D. Vaux (1949), Cascading over the continental slope of water from the Celtic Sea, *J. Mar. Biol. Assoc. U. K.*, *28(3)*, 719–750.

Curry, B., C. M. Lee, and B. Petrie (2011), Volume, Freshwater, and Heat Fluxes through Davis Strait, 2004–05*, *J. Phys. Oceanogr.*, *41*(3), 429–436, doi:10.1175/2010JPO4536.1.

Curry, B., C. M. Lee, B. Petrie, R. E. Moritz, and R. Kwok (2014), Multiyear volume, liquid freshwater, and sea ice transports through Davis Strait, 2004–10*, *J. Phys. Oceanogr.*, *44*(4), 1244–1266, doi:10.1175/JPO-D-13-0177.1.

Dukhovskoy, D. S., et al. (2016), Greenland freshwater pathways in the sub-Arctic Seas from model experiments with passive tracers, *J. Geophys. Res. Oceans*, *121*, 877–907, doi:10.1002/2015JC011290.

Fichefet, T., and M. Morales Maqueda (1997), Sensitivity of a global sea ice model to the treatment of ice thermodynamics and dynamics, *J. Geophys. Res.*, *102*, 12,609–12,646, doi:10.1029/97JC00480.

Fratantoni, P., and R. Pickart (2007), The western North Atlantic shelfbreak current system in summer, *J. Phys. Oceanogr.*, *37*, 2509–2533.

Gordon, A. L., A. H. Orsi, R. Muench, B. A. Huber, E. Zambianchi, and M. Visbeck (2009), Western Ross Sea continental slope gravity currents, *Deep Sea Res., Part II*, *56*(13–14), 796–817, doi:10.1016/j.dsr2.2008.10.037.

Haine, T. W. N., et al. (2015), Arctic freshwater export: Status, mechanisms, and prospects, *Global Planet. Change*, *125*, 13–35, doi:10.1016/j.gloplacha.2014.11.013.

Ivanov, V., G. Shapiro, J. Huthnance, D. Aleynik, and P. Golovin (2004), Cascades of dense water around the world ocean, *Prog. Oceanogr.*, *60*(1), 47–98, doi:10.1016/j.pocean.2003.12.002.

Lane-Serff, G. F., and P. G. Baines (2000),Eddy formation by overflows in stratified water, *J. Phys. Oceanogr.*, *30*(2), 327–337, doi:10.1175/1520-0485(2000)030 < 0327:EFBOIS>2.0.CO;2.

Madec, G., and the NEMO Team (2008), NEMO ocean engine, *Note du Pole de Modelisation*, vol. *27*, Inst. Pierre-Simon Laplace (IPSL), France.

Marsh, R., et al. (2015), Nemoicb (v1.0): Interactive icebergs in the nemo ocean model globally configured at eddy-permitting resolution, *Geosci. Model Dev.*, *8*(5), 1547–1562, doi:10.5194/gmd-8-1547-2015.

Masina, S., A. Storto, N. Ferry, M. Valdivieso, K. Haines, M. Balmaseda, H. Zuo, M. Drevillon, and L. Parent (2015), An ensemble of eddy-permitting global ocean reanalyses from the MyOcean project, *Clim. Dyn.*, 1–29, doi:10.1007/s00382-015-2728-5.

Münchow, A., K. K. Falkner, and H. Melling (2015), Baffin Island and West Greenland Current Systems in northern Baffin Bay, *Prog. Oceanogr.*, *132*, 305–317, doi:10.1016/j.pocean.2014.04.001.

Myers, P. G., N. Kulan, and M. H. Ribergaard (2007), Irminger Water variability in the West Greenland Current, *Geophys. Res. Lett.*, *34*, L17601, doi:10.1029/2007GL030419.

Myers, P. G., C. Donnelly, and M. H. Ribergaard (2009), Structure and variability of the West Greenland Current in Summer derived from 6 repeat standard sections, *Prog. Oceanogr.*, *80*(1), 93–112.

Pickart, R. S., D. J. Torres, and P. S. Fratantoni (2005), The East Greenland Spill Jet*, *J. Phys. Oceanogr.*, *35*(6), 1037–1053, doi:10.1175/JPO2734.1.

Punshon, S., K. Azetsu-Scott, and C. M. Lee (2014), On the distribution of dissolved methane in Davis Strait, North Atlantic Ocean, *Mar. Chem.*, *161*, 20–25, doi:https://doi.org/10.1016/j.marchem.2014.02.004.

Rabe, B., P. A. Dodd, E. Hansen, E. Falck, U. Schauer, A. Mackensen, A. Beszczynska-Möller, G. Kattner, E. J. Rohling, and K. Cox (2013), Liquid export of Arctic freshwater components through the Fram Strait 1998–2011, *Ocean Sci.*, *9*(1), 91–109, doi:10.5194/os-9-91-2013.

Rattan, S., P. G. Myers, A.-M. Treguier, S. Theetten, A. Biastoch, and C. Böning (2010), Towards an understanding of Labrador Sea salinity drift in eddy-permitting simulations, *Ocean Modell.*, *35*(1–2), 77–88, doi:10.1016/j.ocemod.2010.06.007.

Shapiro, G. I., and A. E. Hill (1997), Dynamics of dense water cascades at the shelf edge, *J. Phys. Oceanogr.*, *27*(11), 2381–2394, doi:10.1175/1520-0485(1997)027 <2381:DODWCA>2.0.CO;2.

Shapiro, G. I., and A. E. Hill (2003), The alternative density structures of cold/saltwater pools on a sloping bottom: The role of friction, *J. Phys. Oceanogr.*, *33*(2), 390–406, doi:10.1175/1520-0485(2003)033 < 0390:TADSOC>2.0.CO;2.

Shapiro, G. I., J. M. Huthnance, and V. V. Ivanov (2003), Dense water cascading off the continental shelf, *J. Geophys. Res.*, *108*(C12), 3390, doi:10.1029/2002JC001610.

Smith, G. C., F. Roy, P. Mann, F. Dupont, B. Brasnett, J.-F. Lemieux, S. Laroche, and S. Bélair (2014), A new atmospheric dataset for forcing ice-ocean models: Evaluation of reforecasts using the Canadian global deterministic prediction system, *Q. J. R. Meteorol. Soc.*, *140*(680), 881–894, doi:10.1002/qj.2194.

Tang, C. C., C. K. Ross, T. Yao, B. Petrie, B. M. DeTracey, and E. Dunlap (2004), The circulation, water masses and sea-ice of Baffin Bay, *Prog. Oceanogr.*, *63*(4), 183–228, doi:10.1016/j.pocean.2004.09.005.

von Appen, W.-J., I. M. Koszalka, R. S. Pickart, T. W. Haine, D. Mastropole, M. G. Magaldi, H. Valdimarsson, J. Girton, K. Jochumsen, and G. Krahmann (2014), The East Greenland Spill Jet as an important component of the Atlantic Meridional Overturning Circulation, *Deep Sea Res., Part I*, *92*, 75–84, doi:10.1016/j.dsr.2014.06.002.

Wobus, F., G. I. Shapiro, J. M. Huthnance, M. A. M. Maqueda, and Y. Aksenov (2013), Tidally induced lateral dispersion of the Storfjorden overflow plume, *Ocean Sci.*, *9*(5), 885–899, doi:10.5194/os-9-885-2013.